JOURNAL OF MATERIALS SCIENCE 25 (1990) 2642–2653

Electron microscopy of inertia–friction weldments in a rapidly solidified Al–Fe–Mo–V alloy

K. H. HOU, W. A. BAESLACK III
Department of Welding Engineering, The Ohio State University, Columbus, Ohio 43210, USA

The microstructures of inertia-friction weldments in a rapidly solidified, powder metallurgy Al–8.7Fe–2.8Mo–1V alloy were characterized using light and transmission electron microscopy. Extensive plastic deformation at the weld interface during the welding process was shown to fracture and disperse relatively coarse, spherical dispersoids present in the original base-metal microstructure, thereby resulting in a refined dispersoid size in this region. These fine dispersoids promoted an increase in hardness at the weld interface as compared to the unaffected base metal. Local regions of nonuniform interface deformation at the weld outer periphery resulted in a heterogeneous microstructure comprised of adjacent regions of high and low dispersoid density. The dispersoid-lean regions were characterized by appreciably coarsened alpha grains and a hardness well below that of the base metal. The greater extent of dispersoid-lean regions in welds produced with low axial force promoted preferential weld interface failure during three-point bend testing, while the near absence of these regions in welds produced with high axial force promoted failure in the unaffected base metal remote from the weld.

1. Introduction

Dispersion-strengthened aluminium alloys produced by rapid solidification/powder metallurgy (RS/PM) represent an important new class of materials for applications at elevated temperatures up to 350° C [1]. These alloys are basically hypereutectic Al–Fe compositions with ternary and quaternary alloying additions of cerium, molybdenum, silicon and vanadium to improve room-temperature strength and ductility and elevated-temperature creep properties. Through rapid solidification processing, the formation of coarse, primary intermetallics is suppressed and solidification instead occurs to primary alpha aluminium. Subsequent powder consolidation and thermo-mechanical processing promote the formation of a high volume fraction of thermally stable strengthening phases in a matrix of submicrometre alpha grains. This unique microstructure has been shown to provide high room-temperature strength and elevated-temperature mechanical properties previously not obtainable in conventional, ingot-metallurgy aluminium alloys [1]. The use of dispersion-strengthened RS/PM aluminium alloys in structural applications as potential replacements for conventional aluminium and titanium alloys will require their effective and economical joining. Unfortunately, the "engineered" microstructures exhibited by these alloys generally preclude their joining using conventional fusion welding techniques. Rather, joining processes must be utilized which can effectively "recreate" and/or "retain" in the weld region the unique microstructures upon which these alloys depend for their superior mechanical properties. Both fusion and solid-state joining processes have demonstrated a potential for achieving these goals. Such joining processes include electron-beam and laser welding [2–4], capacitor-discharge welding [5, 6] diffusion welding [7] and inertia-friction welding [8].

The successful fusion welding of RS/PM aluminium alloys requires rapid solidification and cooling rates which can prevent fusion zone solidification to undesirable, near-equilibrium microstructures and minimize microstructural coarsening and softening in the adjacent weld heat-affected zone. Electron-beam and laser welding studies on low hydrogen level RS/PM Al–8Fe–2Mo sheet have determined that the rapid solidification/cooling rates associated with these processes promote the formation of RS fusion zone microstructures exhibiting hardnesses and strengths superior to that of the base metal with minimal dispersoid coarsening in the heat-affected zone (HAZ). Joint efficiencies up to 100% have been achieved in Nd : YAG laser welds [4] which cool at rates approaching 10^5° C sec^{-1}. Despite this capability to "recreate" an RS weld zone microstructure, fusion welding techniques have been applied with limited success to Al–Fe–X alloys because of the inherently high hydrogen content of RS/PM aluminium alloys and the associated formation of fusion zone porosity. Studies by the authors [5, 6] involving an RS/PM Al–Fe–Ce alloy containing a high hydrogen content have shown that high pressures experienced during fusion zone solidification in capacitor-discharge welds can prevent porosity formation while promoting the formation of an RS fusion zone. However, geometric and size

0022–2461/90 $03.00 + .12

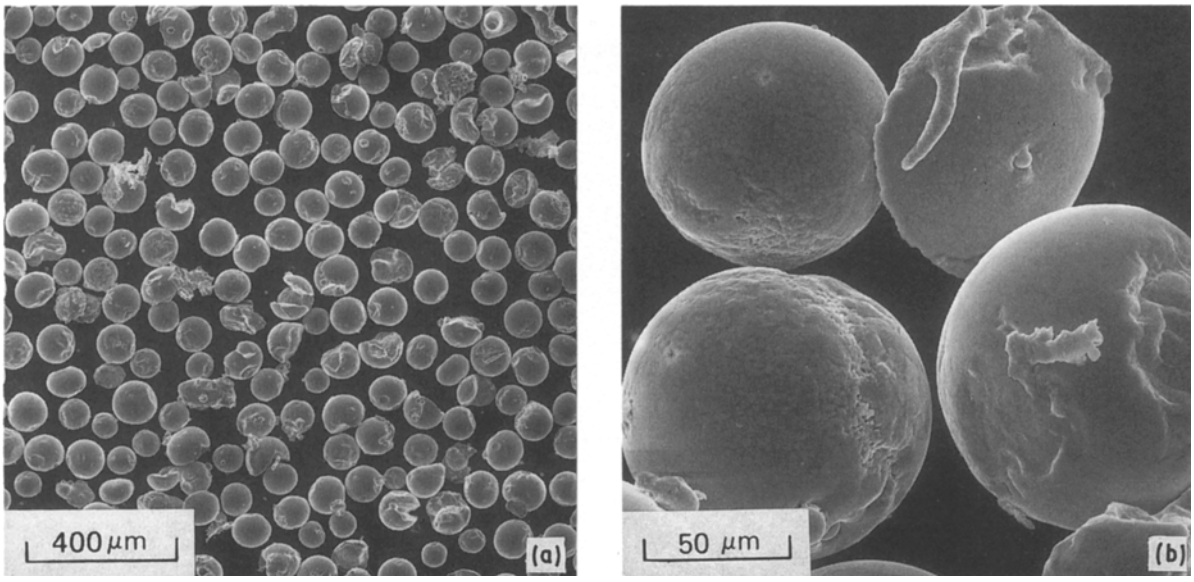

Figure 1 Scanning electron micrographs of Al–Fe–Mo–X rotary-atomized powder.

limitations of parts joined by this process restrict its utility.

Solid-state welding processes offer an important alternative to the fusion welding of Al–Fe–X alloys because both melting and solidification are avoided. Inertia-friction welding is a solid-state joining process that combines frictional heating generated at the faying surfaces with a high axial force to produce a metallic bond [9]. The general absence of melting at the interface during this process eliminates solidification-related discontinuities such as porosity and cracking. Also, the expulsion of surface contaminants and heat-and-deformation-affected metal at the weld faying interfaces during the forging stage of the process promotes final coalescence between nearly unaffected base materials. Inertia-friction welding studies on high-hydrogen content Al–Fe–Ce alloys [8] found that a high axial force promotes the formation of high-integrity, defect-free bonds which exhibit joint efficiencies exceeding 80%. Analysis of the weld interface region using light and scanning electron microscopy (SEM) revealed an extremely fine, complex microstructure which evolved from the complex nature of the thermal and mechanical conditions experienced during the steady state and final forging stages of the welding process. Unfortunately, the limited spatial resolution of the microscopy techniques utilized in this original study precluded thorough microstructure characterization and therefore limited the development of structure/property/fracture relationships.

The principal objective of the present study was to characterize in greater detail the weld interface microstructure of inertia-friction welds in a RS/PM Al–Fe–V–Mo aluminium alloy using thin-foil electron microscopy techniques.

2. Experimental methods

2.1. Materials

The chemical composition of the RS/PM Al–Fe–Mo–V alloy studied in the present investigation (in wt %) was Al–8.7Fe–2.8Mo–1.0V.

Powder production and processing were performed by Pratt and Whitney Aircraft using a rotary atomization (RSR) process [10]. Forced convective cooling with helium provided liquid droplet cooling rates of between 10^4 and $10^{6\circ}$ C sec^{-1} and minimized surface oxide and hydrate formation. Fig. 1 illustrates the spherical powder particles typically produced with

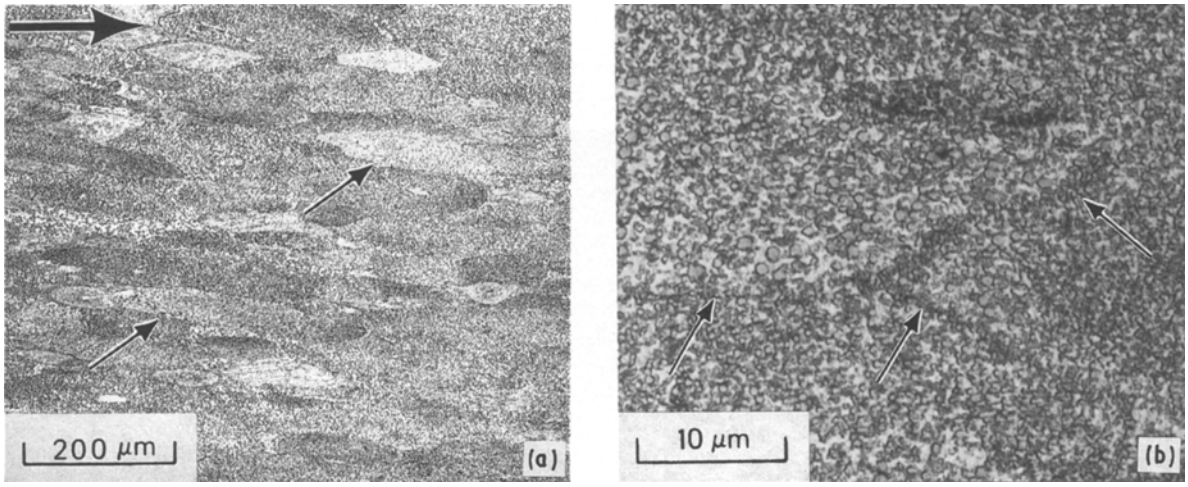

Figure 2 Light micrographs of Al–8.7Fe–2.8Mo–1V extrusion. Large arrow in (a) indicates extrusion direction, small arrows in (a) and (b) indicate powder particle boundaries.

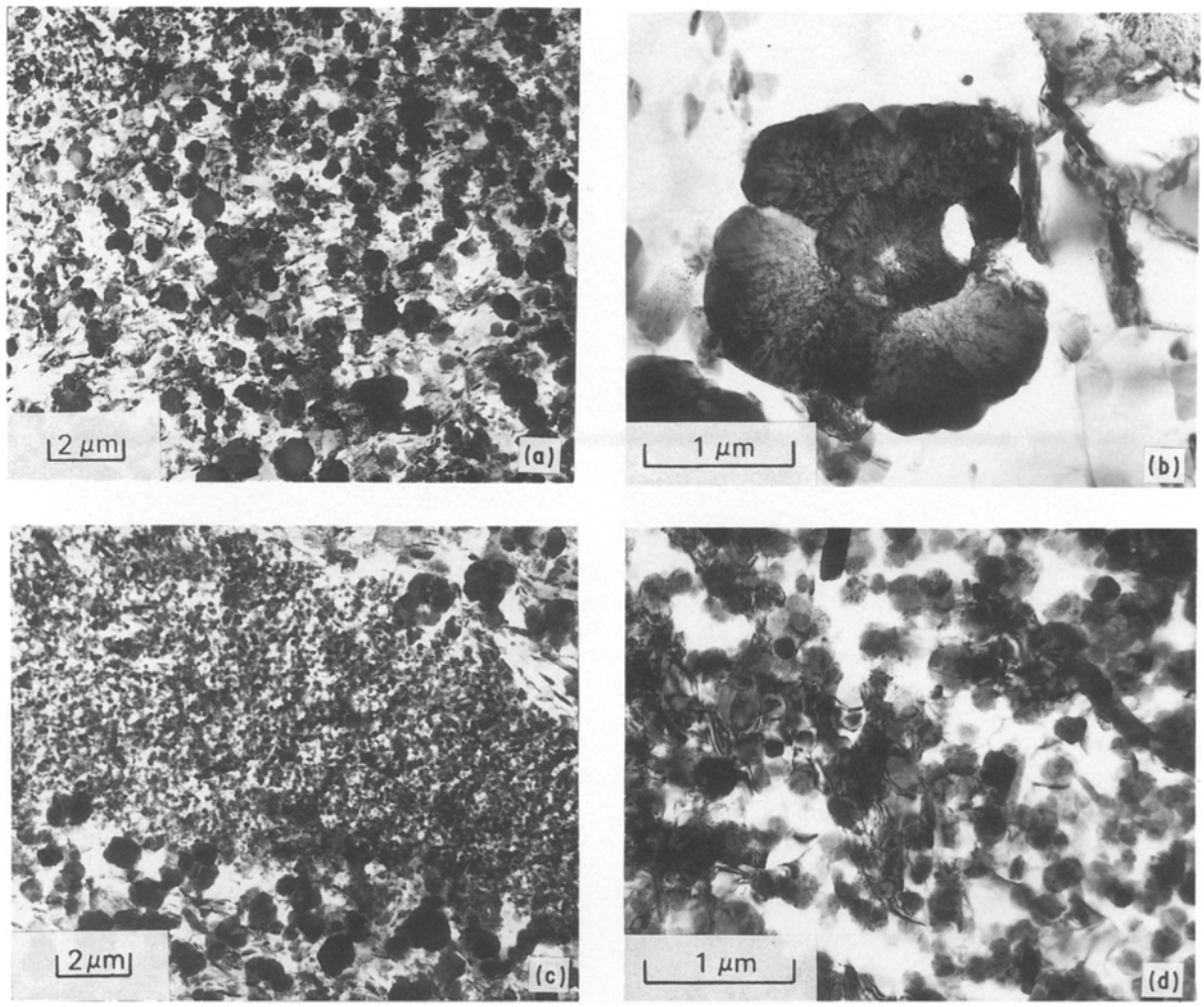

Figure 3 TEM bright-field micrographs of Al–8.7Fe–2.8Mo–1V extrusion: (a, b) predominant microstructure; (c, d) elongated region exhibiting fine dispersoid structure.

this atomization process. Powder particle diameters range from about 25 to 100 μm.

Subsequent to atomization, powders were screened, hot vacuum degassed and extruded to a 250 mm diameter cross-section. Despite atomization and consolidation under completely inert conditions, the final product exhibited a hydrogen content sufficiently high to promote unacceptible levels of porosity in gas tungsten-arc fusion weldments. Cylindrical specimens 22.2 mm diameter and 50.8 mm long were dry machined from the extrusion with the specimen longitudinal axis along the extrusion direction. Prior to welding, each specimen surface was mechanically ground and cleaned with acetone.

2.2. Inertia-friction welding

Inertia-friction welds were produced on an MTI Model 120 inertia-friction welding system. Principal welding parameters, including the moment of inertia, rotational speed and axial force were determined from previous work [8]. These parameters were further optimized in preliminary welding trials which evaluated weld quality strictly from visual analysis of the metal flash and axial displacement. Optimized inertia-friction

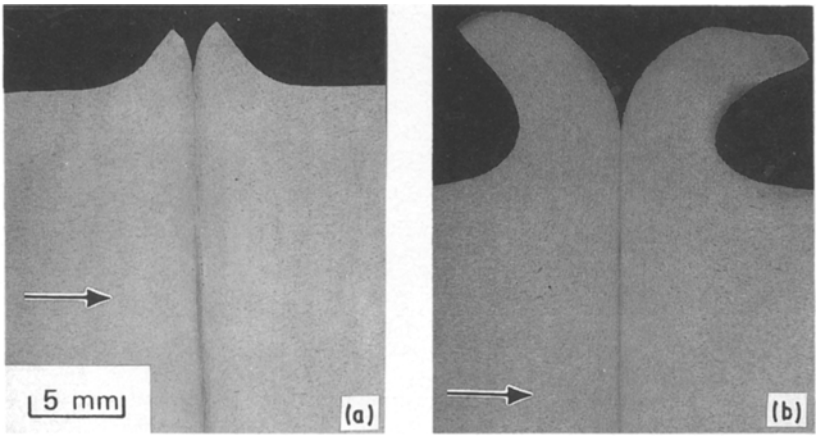

Figure 4 Light macrographs of inertia-friction welds produced in Al–8.7Fe–2.8Mo–1V with (a) low and (b) high axial force. Arrows indicate axial centreline.

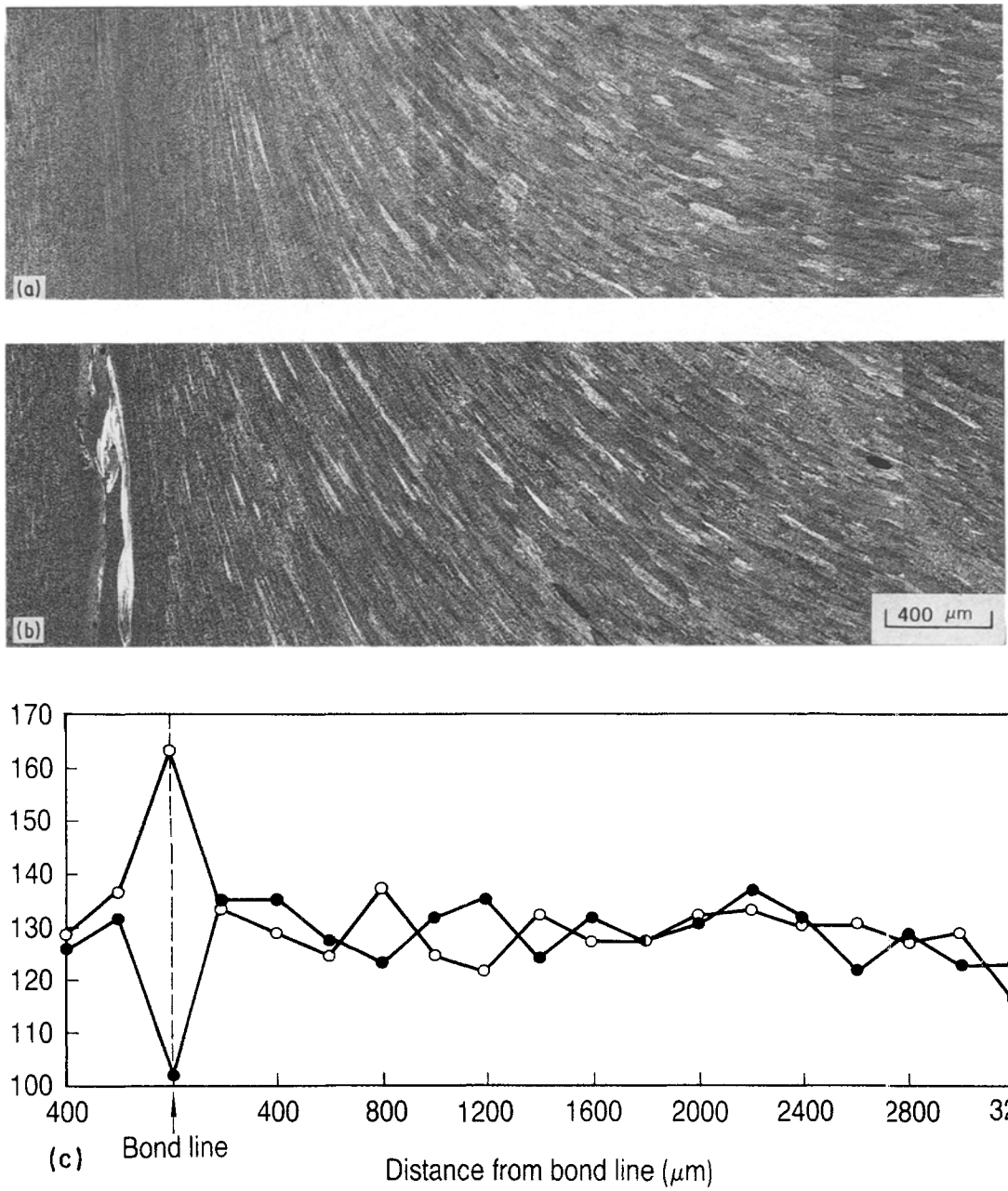

Figure 5 Light macrographs of the (a) centre and (b) outer periphery regions of an inertia-friction weld produced in Al–8.7Fe–2.8Mo–1V with low axial force and corresponding DPH hardness traverses (c). (○) Centre, (●) Outer periphery.

welding parameters were 0.29 kg m^2 moment of inertia, 471 rad sec^{-1} rotational velocity, 126 kN axial force. As mentioned above, axial force had been shown to be very important in achieving an optimum weld zone microstructure and mechanical properties. Therefore, in addition to the "optimized" weldment produced at a "high" axial force, weldments were produced at a "low" axial force of 44.5 kN for comparative evaluation.

2.3. Weld characterization

The principal objective of the present work was to characterize in detail the nature of the weld interface microstructure using thin-foil electron microscopy techniques. Additional analyses performed to complement the electron microscopy analysis included conventional light microscopy, microhardness testing, bend testing and SEM fractographic analysis.

Representative "low"- and "high"-pressure inertia-friction welds were sectioned axially, mounted in epoxy and mechanically polished in a colloidal silica suspension. Following defect analysis of the as-polished specimen surface using light microscopy, microstructural characteristics were revealed by etching with Keller's reagent. Specimen "halves" were carefully sectioned longitudinally at the axial centreline into thin slices 0.3 mm thick using a diamond saw and mechanically thinned on SiC paper down to 0.125 mm. Discs of 3 mm diameter were punched from the foils in the unaffected base metal and from the weld interface regions and electrojet thinned in a solution of 25% nitric acid and methanol at −30° C. Thin foils were examined in a Jeol 200CX analytical electron microscope equipped with a Tracor-Northern TN2000 energy-dispersive X-ray analysis (EDS) system. Analysis included principally bright-field microscopy and semi-quantitative EDS analysis. Selected-area diffraction analysis of the metastable phases typically observed in these alloys is very complex and was not a subject of extensive investigation in the present work.

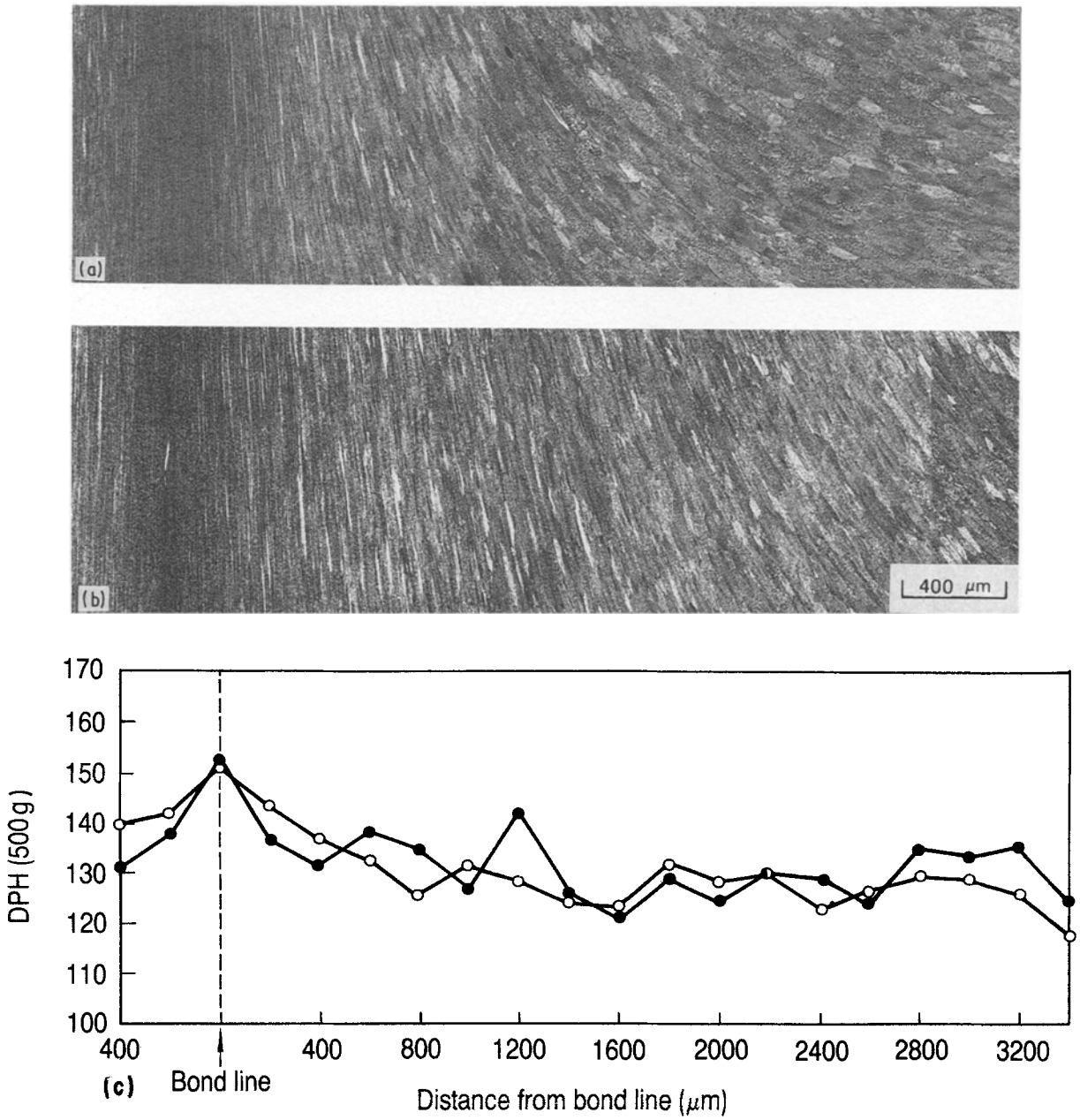

Figure 6 Light micrographs of the (a) centre and (b) outer periphery regions of an inertia-friction weld produced in Al–8.7Fe–2.8Mo–1V with high axial force and corresponding DPH hardness traverses (c). (○) Centre, (●) outer periphery.

Diamond pyramid hardness (DPH) testing was performed across the weld region at the axial centreline and the outer periphery using a load of 500 g and at selected weld interface locations using a load of 50 g. In addition to hardness analysis, three-point bend tests were conducted to identify the preferential failure location in the inertia-friction welded specimens. Bend specimens were produced by removing the weld flash and longitudinally sectioning the weldment into two pieces. Three-point bend testing was performed such that the flat surface (weld centre) was placed in tension. Fractographic examination of the bend specimen fracture surfaces was performed using an ETEC Autoscan scanning-electron microscope.

3. Results

3.1. Base metal microstructure

Although microstructure analysis of the as-solidified powder particles was not performed in the present investigation, previous studies of Al–Fe–Mo type powders produced by rotary atomization have shown that the rapid solidification rates generally prevent primary intermetallic formation and instead promote solidification to primary alpha aluminium with a fine intermetallic structure present at dendrite intersticies [10]. The coarseness of the dendritic structure is dependent on the cooling and solidification rates experienced by the individual powder particles, with increased cooling rates promoting finer dendrite and intermetallic structures and increased supersaturation of alloying elements in the alpha phase. During subsequent consolidation and thermo-mechanical processing, these interdendritic dispersoids coarsen and additional phases may form from the supersaturated alpha matrix, with the nature and extent of this phase coarsening and transformation dependent principally on the thermal cycle experienced during consolidation and thermomechanical processing.

Light micrographs of the Al–8.7Fe–2.8Mo–1V base alloy are shown in Fig. 2. Despite thermomechanical

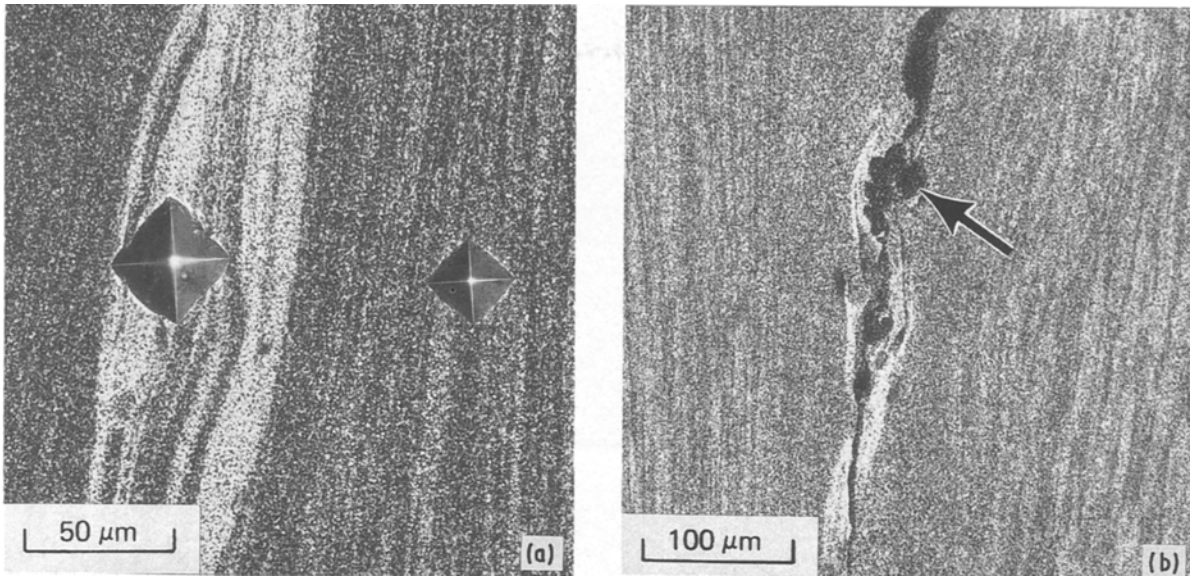

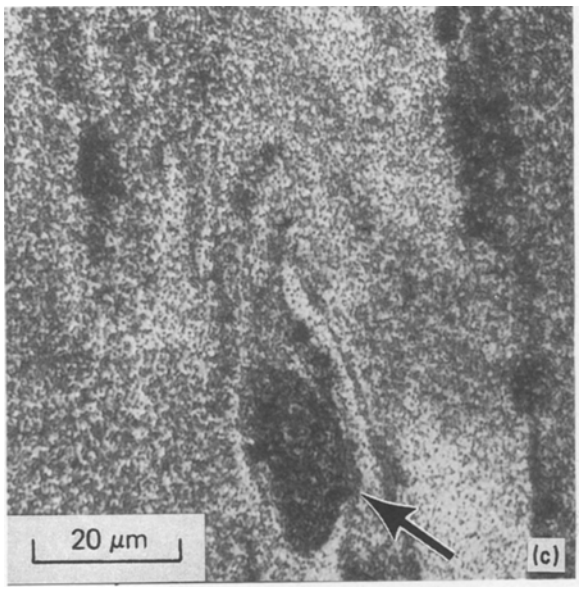

Figure 7 Light micrographs of weld HDZ at outer periphery in inertia-friction weld produced in Al–8.7Fe–2.8Mo–1V with low axial force: (a) DPH microhardness indents produced with 50 g load in adjacent white-etching and dark-etching microstructures; (b, c) very dark-etching regions adjacent to white-etching HDZ.

processing by hot pressing and extrusion, evidence of the original powder particles elongated in the extrusion direction can still be observed. Light microscopy at increased magnification (Fig. 2b) indicated that contrast differences between the particles result from variations in the coarseness of the dispersoid structure within the alpha matrix, with the dark-etching regions exhibiting a high density of fine dispersoids and the light-etching regions exhibiting fewer, coarser dispersoids.

Microstructural characteristics of the base metal were more clearly delineated by transmission-electron microscopy (TEM). As shown in Figs 3a and b, the microstructure consisted predominantly of relatively coarse, nearly spherical intermetallics ranging in diameter from about 500 to 2000 nm in a matrix of submicrometre alpha aluminium grains. Fine, acicular dispersoids ranging in length from approximately 200 to 1000 nm and fine, spherical dispersoids ranging in diameter from about 100 to 250 nm were also located throughout the alpha matrix. Semi-quantitative EDS analysis found the coarse, spherical dispersoids to contain iron, molybdenum and vanadium, while the acicular and small spherical dispersoids contained only aluminium and iron. Analysis of the alpha matrix revealed the presence of aluminium with only a trace of iron. Although detailed selected-area diffraction was not performed on the different dispersoid morphologies, previous electron microscopy and X-ray diffraction analyses of a similar Al–Fe–Mo–V alloy chemistry [11] indicated the coarse, spherical dispersoids to be $Al_{12}Fe_3(Mo, V)$, the acicular dispersoids to be Al_3Fe and the small spherical dispersoids to be Al_6Fe. Elongated regions containing extremely fine dispersoid structures were also occasionally observed in the base-metal microstructure (Figs 3c and d). These regions likely originated from fine powder particles which solidified to an extremely fine dendritic structure or completely to supersaturated alpha aluminium by a partitionless, planar mode of solidification.

3.2. Weldment characterization

3.2.1. Light microscopy analysis

Visual analysis of both the high and low axial force weldments found good symmetry and continuity of flash around the weld circumference. The appreciably greater flash observed in the high compared to the low axial force weld (Fig. 4) was consistent with the higher axial displacement measured for high compared to low axial force (21.9 compared to 3.81 mm, respectively).

Macroscopic characterization of axially sectioned weldments in the as-polished condition revealed occasional lack-of-bonding defects only at the outer periphery of the low axial force welds. No evidence of hydrogen-induced porosity or blistering, or oxide stringers was observed in either of the welds. Heavy etching of the weldments revealed macroscopic heat and deformation zones (HDZs) comprised of a featureless, grey-etching outer region and a dark-etching central region. The dark-etching centre of the HDZs

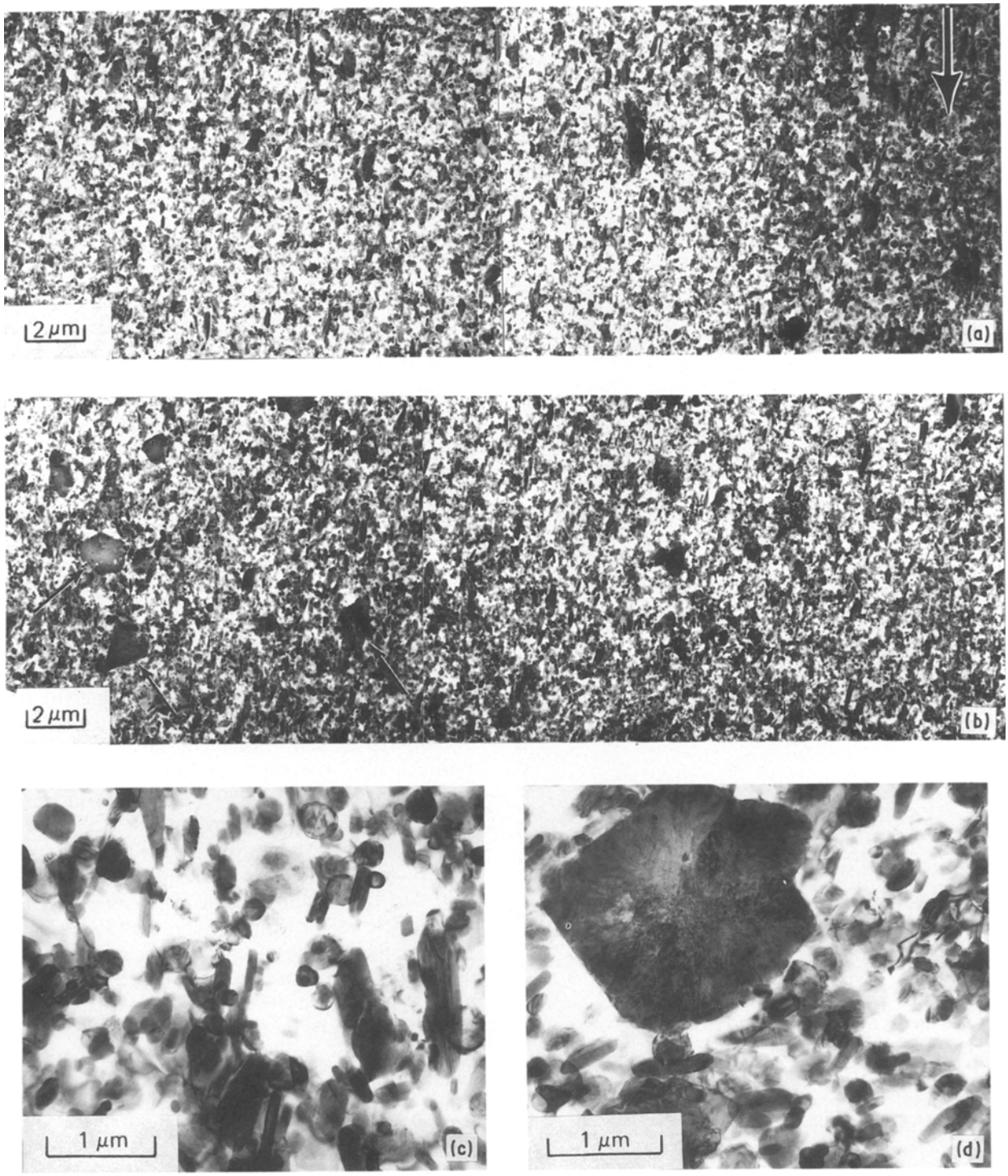

Figure 8 TEM bright-field micrographs of weld interface region at the centre of the inertia-friction weld produced in Al–8.7Fe–2.8Mo–1V with low axial force: (a, b) microstructure traverse across weld region (right side of (b) is continuation of left side of (a)), arrow in (a) indicates location and orientation of weld interface, arrows in (b) indicate angular-shaped coarse dispersoids; (c) interface at increased magnification; (d) angular-shaped dispersoid in (b) at increased magnification.

appeared relatively uniform across the weld and to be slightly wider in the low compared to the high axial force weld.

Light microscopy analysis at increased magnification more clearly revealed the nature of the HDZ regions in both weldment types. Microstructure traverses from the unaffected base metal to the weld interface at the centre and outer periphery of weldments produced at low and high axial force are shown in Figs 5 and 6, respectively. The circumferential, radially outward flow of metal, which is characteristic of inertia-friction welding, was apparent in the outer HDZ. As shown, the microstructure texture across this region continually changed in a uniform manner from parallel to perpendicular to the original base alloy extrusion direction. Nearer to the weld interface, the original base metal microstructure became increasingly "flattened," with the high temperatures and deformation levels directly at the weld interface completely disrupting the base metal microstructure texture and resulting in a uniform, dark-etching microstructure. In general, the width of the entire

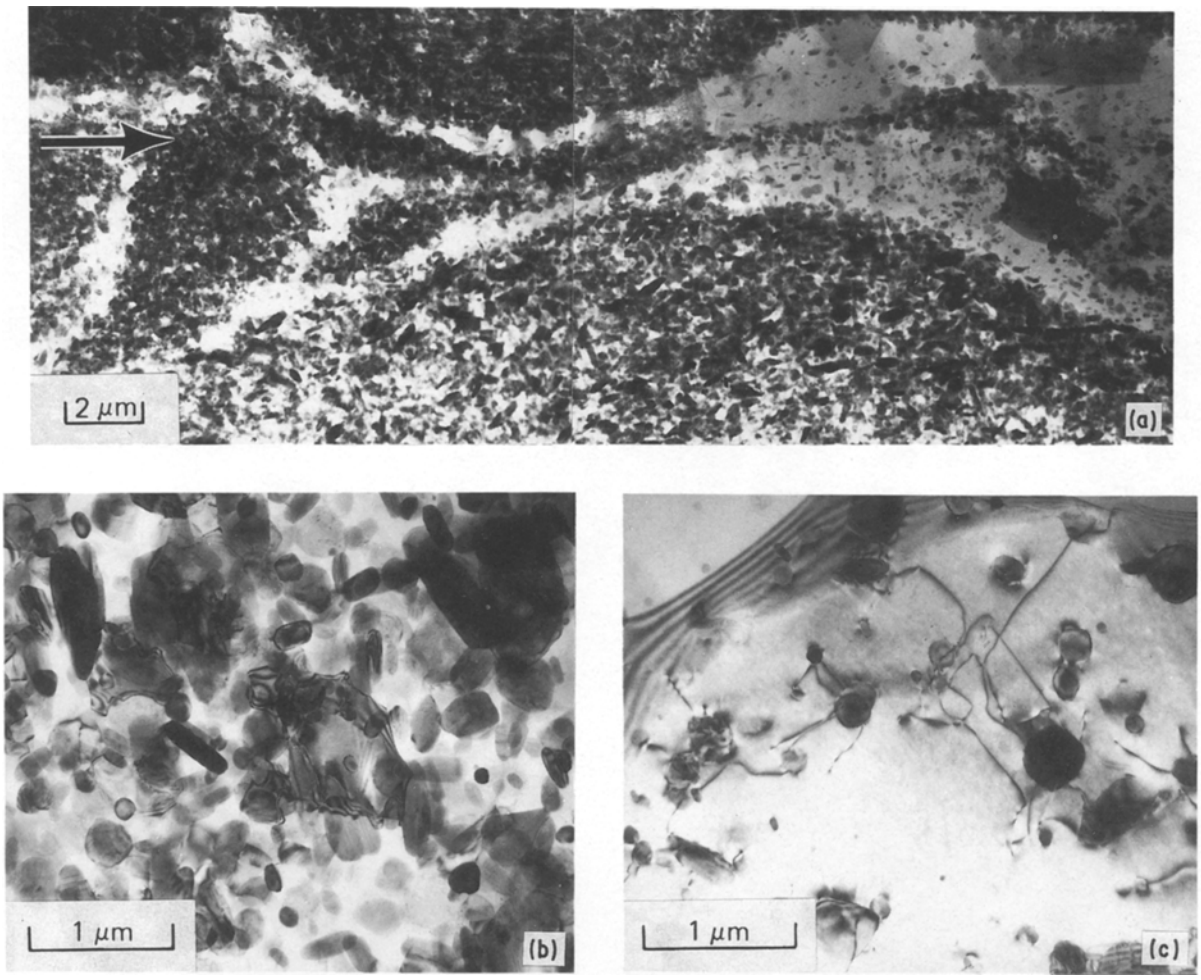

Figure 9 TEM bright-field micrographs of weld interface region at outer periphery of inertia-friction weld produced in Al–8.7Fe–2.8Mo–1V with low axial force: (a) microstructure along weld region, arrow indicates location and orientation of weld interface; (b) region of high dispersoid density at increased magnification; (c) region of low dispersoid density at increased magnification.

HDZ (dark-etching central region and grey-etching outer region in Figs 4a and b) was greater at the outer periphery compared to the weld centreline.

The weld outer periphery regions, particularly in the low axial force welds, commonly exhibited white-etching regions along the weld interface, as shown in Fig. 5b. The analysis of this region at increased magnification suggested a lower dispersoid density compared to the base metal (Fig. 7a). As shown in Figs 7b and c, regions which etched darker than the base metal typically bounded the white-etching regions. Light microscopy indicated a higher dispersoid density in these dark-etching regions as compared to the base metal.

3.3.2. TEM analysis

Transmission electron microscopy was effective in revealing microstructural details of the central HDZ which were unresolvable with light microscopy. Figs 8a and b show a TEM bright-field microscopy traverse at the axial centreline of a weld produced with low axial force from the outer edge of the central HDZ to the weld interface (indicated by the arrow in Fig. 8a). As shown in Figs 8a to c, the region was characterized by a relatively uniform, dense distribution of cigar-shaped dispersoids and lesser quantities of finer acicular and spherical dispersoids, with a near absence of the coarse, spherical dispersoids present throughout the unaffected base metal microstructure. The length, width and specific morphology of the cigar-shaped dispersoids varied locally throughout the microstructure, as shown in Fig. 8c. Interestingly, the cigar-shaped and acicular intermetallics appeared to be aligned nearly parallel to the weld interface (i.e. perpendicular to the applied axial force). EDS analysis showed the cigar-shaped particles and coarser spherical particles to contain aluminium, iron, molybdenum and vanadium in levels comparable to those in the coarse base-metal dispersoids, while the fine acicular particles contained only aluminium and iron. Darker contrast evident at the weld interface resulted from a slightly high density of dispersoids and increased density of dislocations in the alpha aluminium. In correlating the contrast of the light and TEM bright-field micrographs, it is apparent that the uniform, dark-appearing region at the weld interfaces resulted principally from the etching response of the extremely fine distribution of dispersoids present in this region. At distances further from the weld interface (left-hand side of Fig. 8b) the density of coarse intermetallics gradually increased while the proportion of finer acicular and cigar-shaped dispersoids decreased. In contrast to their approximately spherical morphology in the unaffected base metal (Fig. 3b), the coarse dispersoids in the HDZ appeared very angular and faceted (arrows in Figs 8b

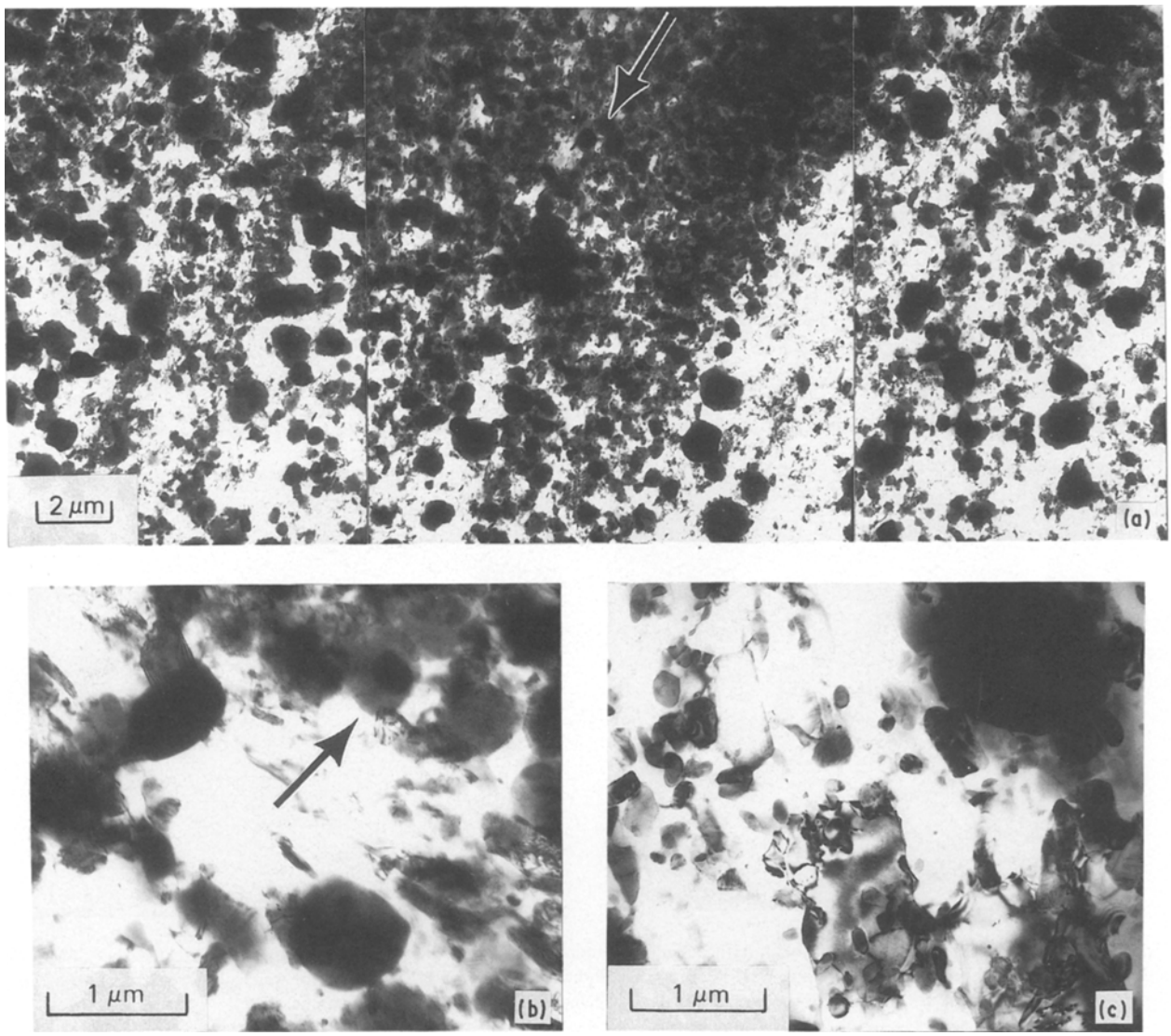

Figure 10 TEM bright-field micrographs of weld interface region at centre of inertia-friction weld produced in Al–8.7Fe–2.8Mo–1V with high axial force: (a) microstructure traverse across weld region, arrow indicates location and orientation of weld interface; (b) region of low dispersoid density at increased magnification; (c) region of high dispersoid density (arrow) at increased magnification.

and d), indicating their partial brittle fracture during welding.

Fig. 9 shows a TEM bright-field traverse along the weld interface at the outer periphery of a weld produced with low axial force. The dark-etching region observed in the light micrograph was comprised of a high density of fine, cigar-shaped and spherical dispersoids (Fig. 9b). with no evidence of the original coarse base-metal dispersoids. Examination of the elongated, white-appearing regions found a very low density of small, spherical dispersoids and occasional cigar-shaped dispersoids (Fig. 8c) in appreciably coarsened alpha grains ranging from 2 to 10 μm diameter. As in the central weld region, the alpha aluminium matrix was found to contain negligible alloying elements while the cigar-shaped and spherical dispersoids contained aluminium, iron, molybdenum and vanadium.

The TEM bright-field microscopy traverse across the weld interface at the centre of a weld produced with a high axial force revealed an appreciably different microstructure compared to that of the low-axial force weld (Fig. 10a). A "striated" microstructure comprised of alternating regions of coarse, spherical dispersoids in a matrix lean in the finer dispersoids (Fig. 10b) and dense mixtures of coarse and fine dispersoids (Fig. 10c) was observed. Further from the interface, the widths of these regions gradually increased as the structure transitioned to that of the unaffected base metal far from the interface.

Fig. 11a shows a TEM bright-field microscopy traverse across the weld zone at the outer periphery of the high axial force weld. A distinct transition was observed from the unaffected base metal microstructure to a region comprised of a high density of fine, spherical and cigar-shaped dispersoids (Fig. 11b). At the particular location shown in Fig. 11, the structure ultimately transitioned at the weld interface to a coarse, equiaxed alpha aluminium grain structure containing a low density of spherical dispersoids (Fig. 11c).

3.3. Mechanical property and fracture analysis

DPH hardness traverses across the high and low axial force inertia-friction welds corresponded well with the observed microstructural characteristics (Figs 5 and 6). In both weld types, significant increases in hardness were associated with the dark-etching, central HDZ regions. This peak hardness rapidly decreased to

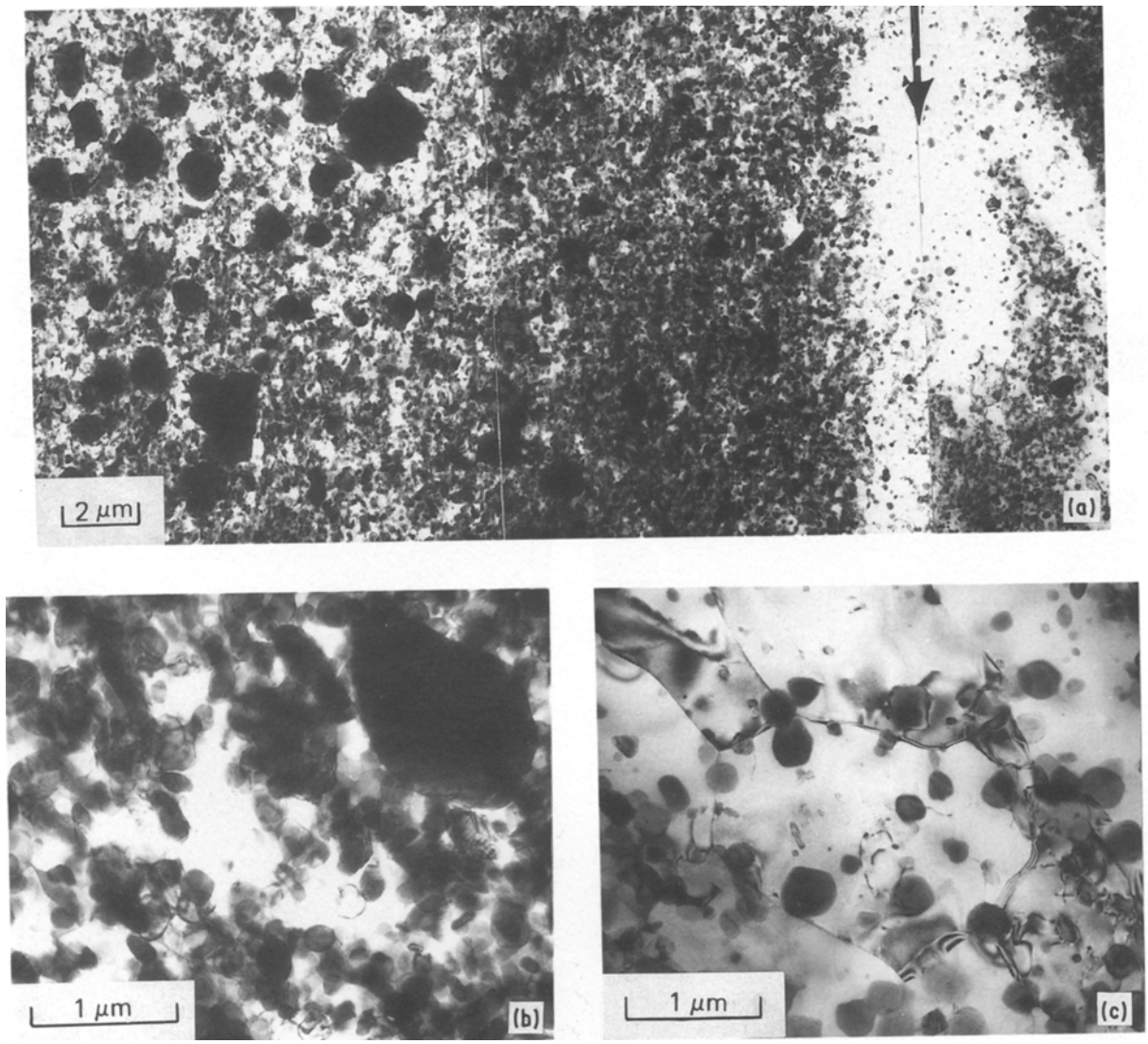

Figure 11 TEM bright-field micrographs of weld interface region at outer periphery of inertia-friction weld produced in Al–8.7Fe–2.8Mo–1V with high axial force: (a) microstructure traverse across weld region, arrow indicates location and orientation of weld interface, (b) region of high dispersoid density at increased magnification; (c) region of low dispersoid density at increased magnification.

base metal hardness levels in the outer HDZ region. Signficant decreases in hardness were observed in the white-etching, low-dispersoid density regions located principally at the outer periphery of low axial force welds. As shown in Fig. 7a, DPH microhardness testing using a low load of 50 g showed appreciable hardness differences between the low dispersoid density and high dispersoid density regions in this outer weld periphery.

Three-point bend tests performed on the high axial force welds failed in the unaffected base metal by a shear-type fracture following appreciable plastic deformation, which was consistent with the higher strength in the weld zone and an absence of fracture-initiating defects. Fracture in the low axial force welds occurred principally along the weld interface with negligible macroscopic deformation.

SEM fractographic analysis of the low axial force weld showed a distinct spiral appearance emanating from the centre of the bar (Fig. 12). As schematically illustrated in Fig. 13, this fracture pattern reflected the effects of the combined torsional and axial forging forces on metal flow experienced at the interface during inertia-friction welding. The fracture surface at the weld outer periphery appeared relatively flat and smooth even at relatively high magnification (Figs 12b and c), which was consistent with the low deformation fracture of this specimen. Near the centre of the bar the fracture path deviated into the far HDZ. Fracture in the far HDZ occurred essentially identical to that in the unaffected base metal by microvoid formation around fine dispersoids and ductile fractile of the soft alpha aluminium matrix (Figs 12d and e).

4. Discussion

Cylindrical specimens welded with the inertia-friction welding process experience complex combinations of axial and torsional forces and stresses across the weld interface [12]. As the schematic illustration in Fig. 13 shows, the plastic flow of metal heated to high temperatures by frictional heating occurs from the central region to the outer periphery in an outward spiralling pattern. Behind the weld interface, the metal flow is generally quite uniform. However, directly at the weld interface nonuniform mechanical mixing can occur in layers of highly plastic metal on each side of the weld

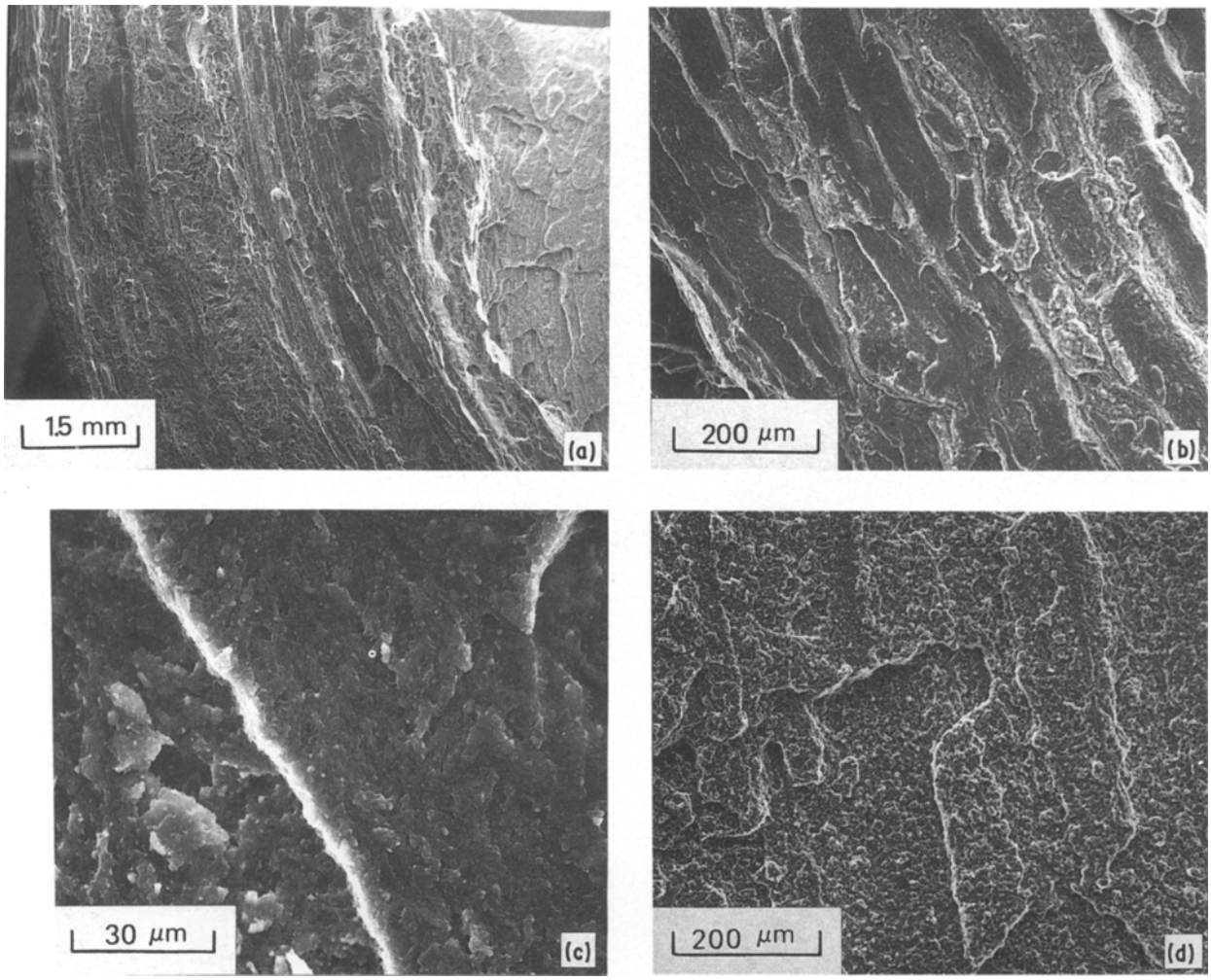

Figure 12 SEM fractographs of low axial force inertia-friction weld bend specimen in Al–8.7Fe–2.8Mo–1V: (a) fracture surface at low magnification; (b, c) fracture surface of outer periphery at increased magnifications; (d, e) fracture surface of central region at increased magnifications.

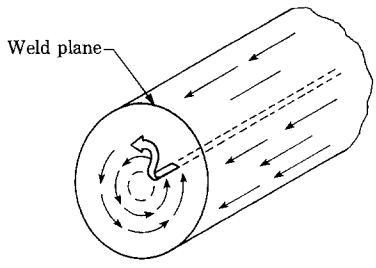

Figure 13 Schematic illustration of metal flow during inertia-friction welding [9].

interface. The final microstructure in the weld interface region is dependent on the nature of this complex deformation.

In the present study, metal flow appeared quite uniform behind the weld interface. In the outer HDZ region, the microstructure texture continuously changed by 90° and was "flattened" by the high compressive stresses in the axial direction. At the weld interface, where temperatures were greatest and local deformation and mechanical mixing most severe, deformation between coarse intermetallics in an extremely soft and plastic alpha aluminium matrix promoted their apparent fracture and dispersion, resulting in the formation of an appreciably finer distribution of cigar-shaped intermetallics. The occurrence of this phenomenon was suggested by the gradual disappearance of the coarse dispersoids in traversing from the unaffected base metal to the central HDZ and the angular appearance of partially fractured dispersoids. This refined dispersoid region was most extensive in the weld produced at low axial force due to the retention of this deformed metal at the weld interface. In the weld produced at high axial force, much of the refined structure was extruded out

of the weld interface region as flash, thereby promoting final bonding between metal less affected by the welding process. Indeed, the appearance of the weld interface microstructure (Fig. 10a) indicates final bonding between severely deformed, but still coherent original powder particles, with the observed microstructure striations resulting from aforementioned variations in the density, size and morphology of dispersoids within different powder particles present in consolidated base-metal microstructure.

Dispersoid-lean regions observed principally in the low-axial force welds originated from localized nonuniform deformation in the interface region. At these locations, high compressive stresses appeared to "extrude" the soft alpha aluminium and some of the finer dispersoids from the original base-metal microstructure. The occurrence of this nonuniform deformation also explains the origin of adjacent regions which exhibit a high density of dispersoids. The near absence of these structures in welds produced with high axial force was related to their extrusion from the weld interface during the final forging stage of the welding process. The large alpha grain size observed in these regions was unexpected because hot working during the welding process and associated dynamic recrystallization would be expected to promote an extremely fine grain size. The nature and density of the dispersoids in this microstructure were apparently insufficient to pin grain boundaries and prevent grain growth during weld cooling.

Based on a previous mechanical evaluation of inertia-friction welds in RS/PM Al–Fe–Ce allows [8], it is expected that the higher hardness associated with the dispersoid-refined central HDZ region and an absence of softening in the outer HDZ would be associated with a higher tensile strength in this region compared to the base metal and a weld joint efficiency of 100%. Although transverse-weld tensile properties were not determined to confirm this supposition, the base metal fracture of three-point bend tests in high axial force welds was consistent with this expected behaviour. The presence of low-strength, dispersoid-lean regions along the weld interface in low-axial force welds represent a significant weld characteristic which may promote tensile fracture along the weld interface at low strength and ductility. Clearly, from the standpoint of optimizing the weldment structure and mechanical properties, weldments should be produced at sufficiently high axial forces to minimize or eliminate the presence of the dispersoid-lean regions at the weld interface.

5. Conclusions

Several important conclusions were obtained from the present investigation.

1. The solid-state inertia-friction welding process was effective in producing high-integrity weldments essentially free of defects.

2. The presence of a refined dispersoid structure in the central heat-and-deformation zone across the weld interface was attributed to the fracture and dispersion of relatively coarse dispersoids present in the original base metal microstructure. This refined dispersoid structure promoted a hardness appreciably greater than that of the unaffected base metal.

3. Nonuniform deformation in the outer weld periphery promoted the formation of dispersoid-rich and dispersoid-lean regions at the weld interface. The dispersoid-lean regions, which were particularly evident in the welds produced with low axial force, exhibited a low hardness and promoted preferential fracture during three-point bend testing along the weld interface. The use of a high axial force minimized microstructural inhomogenieties at the weld interface and promoted fracture during three-point bend testing in the unaffected base-metal region.

Acknowledgements

The authors thank Dr Walter Griffith, AFWAL Materials Laboratory, WPAFB, Ohio, for providing the Al–Fe–V–Mo alloy. They also thank Dr Y. W. Kim, Metcut-Materials Research Group, WPAFB, for helpful comments, Mr Hendrik O. Colijn, OSU Electron Optics Facility, for technical contributions and Dr S. Krishnaswamy for review of this manuscript. Finally, the authors acknowledge support of this work by the Army Research Office, under Contract no. DAAL03-88-0049.

References

1. S. L. LANGENBECK, W. M. GRIFFITH, G. J. HILDEMAN and J. W. SIMON, in "Rapidly-Solidified Powder Aluminum Alloys, ASTM STP 890", edited by E. A. Starke Jr and M. E. Fine (American Society for Testing Materials, Philiadelphia, Pennsylvania, 1986) p. 7.
2. W. A. BAESLACK III and S. KRISHNASWAMY, in "Advances in Welding Science and Technology", edited by S. A. David (ASM International, Metals Park, Ohio 1987) p. 357.
3. S. KRISHNASWAMY and W. A. BAESLACK III, *Mater. Sci. Engng.* **98** (1988) 137.
4. S. KRISHNASWAMY, PhD dissertation, The Ohio State University (1989).
5. W. A. BAESLACK III, K. H. HOU and J. H. DEVLETIAN, *J. Mater. Sci. Lett.* **7** (1988) 944.
6. *Idem, ibid.* **8** (1989) 1716.
7. V. ANANTHANARAYANAN, PhD dissertation, The Ohio State University (1988).
8. W. A. BAESLACK III and K. S. HAGEY, *Weld. J. Res. Suppl.* **67** (1988) 139s.
9. K. K. WANG, "Friction Welding-Welding Research Council Bulletin No. 204", (Welding Research Council, New York, 1975).
10. C. M. ADAM and R. G. BOURDEAU, in "Rapid Solidification Processing, Principles and Technologies II", edited by R. Mehrabian, B. H. Kear and M. Cohen (Claitors, Baton Rouge, 1980) p. 246.
11. S. L. LANGENBECK, R. A. RAINEN, *et al.* in "Elevated Temperature Aluminum Alloy Development", AFWAL-TR-86-4027 (1986) pp. 6–68.
12. M. RAO and T. H. HAZLETT, *Weld. J. Res. Suppl.* **49** (1970) 181s.

Received 14 February
and accepted 24 August 1989